Wind-SST Dipole Mode in the Caribbean and Gulf of Mexico: Large-Scale Features and Drivers

Geidy Rodríguez-Vera (geidyrv@atmosfera.unam.mx)
Universidad Nacional Autónoma de México https://orcid.org/0000-0002-2820-9207
Pedro Ribera
Universidad Pablo de Olavide
Rosario Romero-Centeno
Universidad Nacional Autónoma de México

Research Article

Keywords: Intra-Americas Seas Dipole Mode, wind-SST coupled variability, NASH, Subtropical Jet Stream, NAO, ENSO.

Posted Date: September 29th, 2021

DOI: https://doi.org/10.21203/rs.3.rs-773437/v1

Version of Record: A version of this preprint was published at Climate Dynamics on February 13th, 2022.
See the published version at https://doi.org/10.1007/s00382-021-06093-0.

Abstract

The Dipole Mode (DM) is the leading pattern of springtime wind-SST coupled interannual variability in the Intra-Americas Seas, characterized by SST anomalies of opposite sign between the Caribbean Sea and the Gulf of Mexico. Using the standard deviation (STD) of the wind in a Maximum Correlation Analysis (MCA), this study aims to provide a more dynamic view of the role of the atmosphere in its coupling with the SST. The MCA reveals that the positive phase of the DM is associated with an increase in atmospheric instability, while the negative phase emerges under more stable atmospheric conditions. The DM is preceded by changes in the subtropical high-pressure belt during the previous winter, particularly in the North Atlantic Subtropical High (NASH), and reflects shifts in the latitudinal position of the subtropical jet stream. The DM positive phase tends to occur after an El Niño winter, under negative North Atlantic Oscillation (NAO) conditions. El Niño modulates the DM through a weakening in the meridional pressure gradient and a southward shift of the jet stream. A negative NAO implies a weaker NASH and, therefore, a more irregular circulation over the region. Both El Niño and negative NAO conditions favor the increase in wind STD during the DM positive phase, consistent with an increment in atmospheric disturbances. The DM negative phase responds more to a positive NAO in the previous winter, revealing a stronger NASH acting as an atmospheric block, which justifies the decrease in STD and a more stable circulation.

1 Introduction

The meridional dipole of sea surface temperature anomalies (SSTA) in the Intra-Americas Seas is a natural climate variability pattern most prominent during spring, which has significant interannual fluctuations strongly related to remote influences (e.g., Muñoz et al. 2010; Liu et al. 2015). The dipole consists of SSTA with an opposite sign between the Caribbean Sea and the Gulf of Mexico (CS&GM). This pattern has been observed in the spring following an intense El Niño event (Alexander and Scott 2002). It is also part of the North Atlantic sea surface temperature (SST) tripole, closely associated with the variability of the North Atlantic Oscillation (NAO; Deser et al. 2010). Other studies have reported an equivalent dipole pattern prior to anomalous Western Hemisphere warm pool events (Wang and Enfield 2001; 2003; Enfield et al. 2006). Maldonado et al. (2017) and Martinez et al. (2020) identified a similar configuration of late winter SSTA as a predictor of precipitation in Central America and the Caribbean during the first peak of the rainy season (May-June), especially of extreme precipitation. This SSTA pattern was associated with tropical North Atlantic (TNA) warming during February. Alexander and Scott (2002), Muñoz et al. (2010), and Liu et al. (2015) concur that the SSTA dipole responds mostly to changes in air-sea fluxes, with latent heat flux being the main contributor to this pattern.

Recently, Rodríguez-Vera et al. (2019; hereinafter RV19) observed a seasonal dependence in the patterns of coupled ocean-atmosphere interannual variability in the CS&GM. During March and April, they found a dominant pattern of SSTA, distributed in a dipole-like structure, coupled with surface mean wind anomalies. This pattern, called the Dipole Mode (DM), has a strong resemblance with the meridional dipole of SST in the Intra-Americas Seas. The positive (negative) phase of the DM is considered when the SSTA are positive (negative) in the CS and negative (positive) in the GM. Thus, this paper focuses on the

physical mechanisms associated with the genesis of the leading wind-SST coupled mode in the CS&GM during spring, their large-scale features, and antecedent winter atmospheric conditions.

The climatological wind fields in March-April show the dominant easterlies in the region, more intense within the Caribbean Low-Level Jet core (CLLJ; Amador 1998; Wang 2007), and the CS typically exhibits warmer SST than the GM (Fig. S1a). The DM represents the interannual variability of this SST gradient, which could have implications for the ocean circulation in both basins and the transport through the Yucatan Channel. The standard deviation (STD) of the daily zonal and meridional winds for March-April (the DM months) indicates greater wind variability above 20°N, likely due to the more frequent interaction with mid-latitude synoptic-scale disturbances (Fig. S1b-c). During spring, the northern hemisphere subtropical jet stream moves north of the tropics, and the North Atlantic Subtropical High (NASH) is strengthening and extending its south-western ridge toward the CS&GM region. The subtropical westerly jet stream controls the trajectories of storms and mid-latitude air masses and shows quite persistence concerning the NASH ridge position (Riehl 1962; Schultz et al. 1998). Therefore, we will analyze whether depending on the DM phases there are changes in the position and structure of the jet stream and the NASH.

Particularly, the DM exhibits important connections with the Pacific and Atlantic climate variability (RV19). The DM showed the highest correlations with the NAO and El Niño-Southern Oscillation (ENSO) of the previous winter. Furthermore, the relationship of the DM with both independent teleconnection processes was asymmetric. Frequently in the literature, anomalies associated with large-scale remote patterns, such as ENSO, are presented considering symmetry between their opposite phases (e.g., Alexander and Scott 2002; Lee et al. 2014). However, this work assumes that the effect of opposite phases of teleconnections in the CS&GM is not always symmetrical (e.g., Chikamoto and Tanimoto 2005). In this sense, the insights in RV19 agree with Giannini et al. (2001), who studied the influence of ENSO and NAO on Caribbean rainfall by analyzing different combinations of their phases. They noted that a warm ENSO in combination with a negative NAO has constructive interference in boreal spring.

Understanding the mechanisms by which ENSO and NAO affect the springtime interannual variability of the ocean-atmosphere coupling in the CS&GM region is one of the motivations of this study. First, we further explore the coupling between the wind field and SST in the CS&GM, using the anomalies of the wind STD instead of the mean wind in a multivariate analysis. The aim is to provide a more dynamic view of the role the atmosphere plays in its coupling with the SST. Then, possible changes in atmospheric circulation associated with the generation of the DM will be investigated. Consequently, we propose a more physical sense to the observed asymmetry in the influence of NAO and ENSO on this strong pattern of coupled wind-SST anomalies. The following section includes the data and methods used in this research. The results are presented and discussed in Sect. 3, and a summary and conclusions are provided in Sect. 4. Additional information that supports the present work is included in the supplementary material as Figures S1-S6.

2 Data And Methods

The zonal and meridional components of 10-m winds were taken from the Climate Forecast System Reanalysis (Saha et al. 2010, 2014) with a 0.5° spatial resolution. For SST we use the NOAA Optimum Interpolation product (Reynolds et al. 2007) with 0.25° resolution. To perform statistical computations, the SST data are regridded to a resolution of 0.5° to match point-to-point with the wind data, covering the period from 1982 to 2016. The monthly geopotential height (GPH) is provided by the National Centers for Environmental Prediction-National Center for Atmospheric Research (NCEP/NCAR) reanalysis, with a resolution of 2.5° (Kalnay et al. 1996). Levels of 850 hPa, 500 hPa, and 300 hPa are chosen as representative of the lower, middle, and upper troposphere, respectively. Monthly NCEP/NCAR reanalysis products of temperature, specific humidity, and winds at 850hPa are used to calculate the moisture and temperature advection. From this dataset, monthly surface turbulent and radiative heat fluxes are also included.

For all variables above, the three-month running means and standardized monthly anomalies were calculated considering the study period (1982–2016). The long-term linear trends were subtracted from the data at each grid point, to remove its influence on the interannual variability. The area limited by 9°-31°N and 100°-60°W defined the CS&GM region where the DM was obtained. To investigate the relationship of this pattern with the interannual variability of remote regions, a larger domain bounded by 40°S-60°N and 180°-0°W was chosen, which includes much of the Pacific and Atlantic Oceans.

The DM was previously identified by RV19 as the leading mode of the wind-SST coupled variability in March-April, using a Canonical Correlation Analysis (CCA) between the monthly mean anomalies of the 10m wind and SST. In this study, a Maximum Covariance Analysis (MCA; Barnett and Preisendorfer 1987; Bretherton et al. 1992) between the STD anomalies of both wind components and SSTA for March-April was performed. The MCA identifies pairs of coupled spatial patterns and their corresponding time series through a singular value decomposition of the covariance matrix between two spatiotemporal fields. By introducing the STD of the wind instead of its mean-field into the analysis, the method establishes a more dynamic role of the atmosphere in the coupled air-sea variability. This new perspective allowed us to obtain more information on the nature of the interannual variability of the coupling between the surface wind field and the SST in the CS&GM during spring.

To explore potential associations of the DM with other modes of variability, such as teleconnection patterns, various indices are employed. First, the Dipole Index defined by RV19 from a CCA is used. This index is based on the expansion coefficients of the leading wind-SST coupled patterns for March and April. The classification of DM phases is done via percentiles. For a given year, a value of the Dipole Index above (below) the 80th (20th) percentile indicates a positive (negative) phase of the DM. When the index is between the 40th and 60th percentiles, the DM is considered to be in the neutral phase. The seven most representative years for the DM positive phase are: 1983, 1987, 1993, 1998, 2005, 2006 and 2010; and those for the negative phase are: 1989, 1990, 1997, 2002, 2008, 2014, 2015. Using the same criteria, the seven years with the most positive (1989, 1990, 1997, 2000, 2014, 2015, 2016) and negative (1983, 1985, 1986, 1987, 2006, 2007, 2010) NAO and the most intense El Niño (1983, 1987, 1992, 1995, 1998, 2010, 2016) and La Niña (1985, 1989, 1996, 1999, 2000, 2008, 2011) events were extracted, based on the North

Atlantic Oscillation Index (NAOI) and the Oceanic Nino Index (ONI) of the Jan-Feb-Mar quarter (JFM), respectively.

Other climate indices included in this study are the Pacific-North American Index (PNAI) and the Tropical Northern Atlantic Index (TNAI). The PNAI describes the monthly evolution of the Pacific-North American teleconnection pattern (PNA; Barnston and Livezey 1987). The TNAI consists of the anomaly of the monthly SST average between 5.5°-23.5°N and 57.5°-15°W. NAOI, ONI, and PNAI were obtained from the NOAA's Climate Prediction Center (https://www.cpc.ncep.noaa.gov/), and TNAI from the NOAA ESRL Physical Sciences Laboratory (http://psl.noaa.gov).

Additionally, this study employs the database of jet streams developed by Peña-Ortiz et al. (2013). This product provides the frequency of occurrence of local maximum horizontal winds above 30 m/s between 400 hPa and 100 hPa, as the probability of jet cores at each grid point. Figure S1 includes the climatology of the jet cores during the boreal spring for the period 1982–2016. Hence, we will obtain composites of anomalies from these jet conditions.

Using the information of the Dipole Index, ONI, and NAOI, composites of GPH anomalies and jet streams were constructed for the different phases of each oscillation. To further investigate the interannual behavior of SST and zonal and meridional winds as well as their relationship with other climatic events, timeseries for the GM and the CS were constructed independently, by averaging the March-April anomalies within the boxed areas shown in Fig. 1c. Correlations with teleconnection indices are first calculated for the entire period from 1982 to 2016 and then filtering only for the DM years (those that coincide with a positive or negative phase of the DM).

3 Results And Discussion

a. Dipole Mode and wind variance

Analysis of climate patterns is often done using mean fields anomalies. However, here we propose a further analysis to better understand the influence of the surface wind on SSTA, which does not define a static configuration of the anomalous atmospheric circulation as the mean wind does. In this case, the anomalies of the STD of the zonal and meridional winds can provide a more dynamic approximation, one that does consider the disturbances that affect the mean wind and hence facilitates the physical interpretation of the coupling patterns. In this way, low values in the STD fields would indicate a predominance of the mean wind over the wind-SST coupling. On the contrary, higher values of the STD fields indicate that the wind speed or direction is more variable and, thus, the mean value of the wind is less representative, and its variations are the ones that exert a greater influence on the wind-SST coupling.

In accordance with the above, we conducted a MCA using the interannual anomalies of SST and the STD of both wind components. The MCA leading mode explains 31% of the covariance between SSTA and wind STD anomalies. The heterogeneous regression maps reveal that positive anomalies of the wind

STD (Fig. 1a-b) are coupled with a SSTA pattern analogous to the DM (Fig. 1c), which was previously obtained through the CCA using the mean wind anomalies (RV19). Therefore, the SSTA dipole is very consistent and robust, as it emerges from both the CCA, using the mean wind anomalies, and the MCA, using the anomalies of the wind STD. The wind STD anomaly fields (Fig. 1a-b) show an increase in wind variability over almost the entire domain, in phase with years having a positive value of the expansion coefficient. In the GM, this greater wind variability is mainly related to anomalies of the zonal wind variance (Fig. 1a), while in the CS an increase in the variability of the meridional wind predominates (Fig. 1b).

The corresponding expansion coefficients for SST and wind STD of the MCA leading mode are shown in Fig. 1d. They exhibit a significant correlation of 0.80, suggesting a strong coupling. The MCA Index consists of the average between this pair of time series (like Handoh et al. 2006). The interannual variability of the MCA and Dipole indices are also comparable (Fig. 1d), with a significant correlation of 0.85. Both the MCA and the Dipole indices can be considered as a very accurate representation of the Dipole Mode. We verified that the analyzes carried out using the Dipole Index of RV19 or the MCA Index yield very similar results to each other and reflect the same mode of variability, so the interpretation and discussions apply to both cases. Hence, in the subsequent figures we show the results obtained using the Dipole Index of RV19 to facilitate comparison with the previous work.

Anomaly composites of the mean wind field have a strong signal in the CLLJ region, indicating that the DM is closely related to the interannual variability of this important wind system in the CS, where the mean wind speed reduces (intensifies) during the positive (negative) DM (Fig. 2). The MCA further indicates that this is associated with an increase (decrease) in atmospheric variability reflected mainly in the meridional wind. In other words, greater instability in years with a DM positive (negative) phase leads to a decrease (increase) of the persistence of the easterly winds and warming (cooling) in the CS. On the other hand, for the GM the increase (decrease) of zonal and meridional winds variability coincides with a colder (warmer) SST (Fig. 2). Northwesterly wind anomalies cover most of the GM in the positive phase of the DM; but, in general, the mean wind speed does not exhibit significant anomalies, except in the northeast of the GM, the Florida Peninsula and adjacent Atlantic (Fig. 2). This implies that the mechanisms involved in air-sea coupling at the CS differ from those at the GM. For the negative phase of DM, the SSTA pattern appears to be less marked and less significant, except in the northernmost Atlantic region of the domain (Fig. 2). In the following subsections, we will explore the antecedent conditions, some large-scale modulators, and the physical mechanisms involved in this ocean-atmosphere coupling.

b. Evolution of the Dipole Mode and atmospheric drivers

The mean life cycle of the DM from the previous winter to next summer is shown in Fig. 3 through the wind and SST anomalies associated with the Dipole Index. The DM seems to be strongly linked to the SSTA variability in the equatorial Pacific during the boreal winter and to subsequent warming of the TNA. This is consistent with earlier studies that pointed out the increase of the TNA SST about three to five months after a mature phase of El Niño event, in combination with a decrease of the trade winds speed

and the surface heat fluxes release from the ocean (Curtis and Hastenrath 1995; Enfield and Mayer 1997; Saravanan and Chang 2000; Chiang and Sobel 2002; Wang and Enfield 2003). The weakening of the low-level winds in the TNA leads to a decrease in the cooling of the surface by evaporation and upwelling due to the advection of the surface water, resulting in positive SSTA, and conversely. The anomalous wind pattern in the North Atlantic from peak winter through spring suggests a connection with the NASH circulation. Moreover, from JFM to AMJ the cold SSTA in the GM and the subtropical North Atlantic in conjunction with the warming in the TNA and the subpolar North Atlantic (above 40°N) allude to the SST tripole associated with NAO (Desser et al. 2010). Hence, the distribution of wind-SST anomalies associated with DM, especially in CS, suggests that these are linked to a larger scale coupled pattern that comprises the entire TNA since late winter and persists for several months after the mature DM.

The large-scale nature of the DM triggers is also evident in the temporal evolution of the correlations of GPH anomalies at different pressure levels with the Dipole Index (Fig. 4). Since the peak winter, a trough-shaped pattern stands out in the negative correlations, which connects two cores of maximum correlations, on both sides of the North American continent, one in the North Pacific around 40°N and the other in the North Atlantic around 30°N approximately. This pattern reinforces, in effect, the suggestion of a link with the north belt of high subtropical pressures, especially with the NASH, and possibly with the descending branch of the Hadley cell. The negative correlation pattern is bounded by positive correlations to the north side and a wide zone in the middle and upper atmosphere around the region between 20°N and 20°S.

During DJF through FMA, in the CS region, positive correlations are observed between the Dipole Index and the GPH anomalies at the middle and upper troposphere, whereas near the surface the correlations are negative (Fig. 4). Such correlation patterns over the CS correspond to GPH anomalies that have an impact on the vertical wind shear, so that for the positive DM the wind shear decreases, which is consistent with the wind speed reduction and the westerly wind anomalies along with the surface warming in the CLLJ region (Figs. 2–3). The opposite would apply for the negative DM. Similar anomalies in the vertical GPH distribution, and therefore in the wind shear, associated with warmer/colder TNA SST zones in February, were obtained by Maldonado et al. (2017), with an impact on the tropical convection and the Central American precipitation during May-June, the early rainy season. Meanwhile, the GPH negative correlations across the vertical column over the GM, suggest that the physical mechanisms in the GM involved in the ocean-atmosphere coupling that triggers the DM are different from those in the CS (Fig. 4).

The GPH anomaly correlations described above continue during MAM (not shown), and by AMJ although the trough-shaped pattern disappears, the bands of positive correlation at the middle and upper troposphere and the negative correlation near the surface still prevail (Fig. 4). The patterns of wind and SST anomalies on the TNA also tend to remain after spring (Fig. 3). In other words, the persistence of these GPH, SST, and winds anomaly signals for several months suggests that the DM variability might be of importance to modulate climate anomalies into CS&GM and adjacent continent throughout the next summer. It has been proposed that TNA SSTA interannual variability can be used as a good predictor for

the precipitation anomalies at the early rainy season in the CS and Central America (Taylor et al. 2002; Alfaro 2007; Maldonado et al. 2017). Recently, Martinez et al. (2020) pointed out that dry early rainy seasons in the CS are strongly associated with a preceding winter-spring SSTA pattern compatible with the negative phase of the DM, positive sea level pressure anomalies over the TNA, and a positive NAO. The inverse signals are expected to precede the wet early rainy seasons.

Heretofore, the results show sufficient evidence about the importance of the preceding winter atmospheric circulation for DM development. The antecedent winter conditions are explored in more detail using the GPH composites for the positive and negative phases of the DM at 500hPa (Fig. 5). In these panels, a zone of significant anomalies into the North Pacific connected with the southwest flank of the NASH highlights, which is consistent with the two cores of maximum correlations on both sides of North America previously mentioned (Fig. 4). Anomalies associated with the North Pacific core are more significant for the positive than for the DM negative phase. This denotes that the interannual variability of the Pacific side during the previous winter takes greater importance for triggering the positive DM. The significant GPH anomalies associated with the Atlantic core are opposite in sign between the extreme phases of the DM so that negative (positive) GPH anomalies over the CS&GM are expected in the winter before the positive (negative) DM (Fig. 5).

Mean conditions at 850 hPa do show a weak (strong) and less (more) expanded NASH towards GM during winter (not shown) before the positive (negative) DM, and these patterns persist into springtime (Fig. 6). Significant changes in the NASH intensity and extension involve strengthening/weakening of the meridional pressure gradient between the tropics and subtropics. This may explain the response of the North Atlantic trade winds as gleaned from Fig. 3, and the anomalies in wind speed observed over the CS during the DM extreme phases (Fig. 2). It is argued that weak (intense) trade winds are associated - through hydrostatic processes such as mixing and evaporative heat lost- with warmer (colder) SST and lower (higher) atmospheric pressures (Curtis and Gamble 2016). Figures 2, 3, and 6 corroborate that these wind-SST-pressure relations are valid for the CS domain, and could imply the deceleration (acceleration) of the warm water advection towards the GM, which also weakens (intensifies) the upwelling in the CS. In turn, the strengthening and westward extension of the NASH has an indirect impact on SSTA of the GM, via counteracting the entry of cold and dry continental air into this region (Reding 1992). This argument agrees with the changes in the wind variance estimated by the MCA such that during the DM positive phase a weakened NASH over the region coincides with greater wind STD, which could be associated with the more frequent passage of mid-latitude systems. A reverse situation occurs during the DM negative phase.

Although the NASH exerts a high control in the climate of the CS&GM, the north-south migration and frequency of cold air masses that reach such latitudes are closely modulated by the location of the subtropical jet stream (Schultz et al. 1998). Patterns of jet streams for the DM positive and negative phases show very different pictures from each other (Fig. 7). During the positive phase, there is a significant increase in the subtropical jet core frequency around 25°N above Mexico, GM and Florida, and a weakened double jet structure compared with the mean conditions (Fig. S1d). During the negative

phase, the jet core is more frequently split into two branches, one over Northeast America north of 40°N and the other over the Atlantic Ocean along the 20°N vicinity.

The panels of significant anomalies in the jet core frequency (second row in Fig. 7) show a marked latitudinal shift of the jet branch that passes through North America, further south during the DM positive phase and further north during the negative phase. These changes in jet location alter prevailing wind patterns and affect the storm tracks such that they reach the southern United States and the GM more (less) frequently during the DM positive (negative) phase. The higher (lower) frequency of storm passage over the region is consistent with an increase (decrease) in wind variability and, therefore, in its STD. Also, this modification of the jet stream justifies the anomalous cooling (warming) in the GM and the smaller (greater) influence of the NASH on the CS&GM during the DM positive (negative) phase (Figs. 2 and 6).

Composites of moisture and temperature advection at 850hPa and turbulent air-sea heat fluxes are provided to support the dynamical analysis (Fig. 8). Latent heat flux is dominant compared to sensible heat flux, and both show significant changes only for the positive phase of DM. The atmosphere at low levels also presents a dipole pattern of significant anomalies in specific humidity and temperature for the DM positive phase, and an opposite pattern in humidity is reflected in the negative phase (Fig. S2). Apparently, in the negative DM, the air-sea differences are not sufficient to reflect a significant change in the turbulent fluxes. On the other hand, the radiative fluxes for the positive DM tend to oppose between them, and they have a negligible impact during the negative DM (Fig. S2). Thus, the net radiative heat flux (shortwave plus longwave radiation) plays a minor role in the SSTA associated to the DM pattern.

The bulk formula for the turbulent fluxes depends on the wind speed and the air-sea difference in temperature and specific humidity (Enfield and Mayer 1997; Alexander and Scott 2002). The nature of the air-sea coupled anomalies in the CS associated with the DM positive phase seems to be quite comparable to that of the deep tropics, where the wind forcing plays a dominant, but not exclusive, role in the generation of heat fluxes via evaporation, and consequently leading to SSTA (Seager et al. 2000; Mahajan et al. 2010). This mechanism can be explained by the wind, evaporation, and SST feedback (e.g., Xie and Philander 1994). The wind composites highlight the sensitivity of this field in the CS to the phase change of the DM (Fig. 2), and these wind anomalies can be strongly modulated by the interannual variability of the NASH (Fig. 6). In contrast, in the GM the heat loss that occurs in the positive DM seems to respond more to the influence of continental air masses that have an impact on the specific humidity and temperature difference between the atmosphere and the ocean. This is confirmed by the temperature and moisture advection anomalies over the GM (Fig. 8). During the DM positive phase, dry and cold air advection take place in the GM and southern United States; and during the negative phase the pattern is opposed, but the anomalies are significant in a smaller area.

Since the springtime SSTA dipole in the Intra-Americas Seas and the coupled DM have been associated with the variability of NAO and ENSO in previous winter (e.g., Alexander and Scott 2002; Muñoz et al. 2010; RV19), in the next section we will further analyze the relationship between both large-scale patterns and the coupled DM signal.

c. Dipole Mode teleconnections

Table 1 summarizes the maximum correlations (R) of the MCA and the Dipole indices with previous NAOI and ONI, as well as with the TNAI for the following months. As mentioned above, the results using both the MCA and the Dipole indices are very consistent with each other. The DM showed maximum correlations, in absolute values, with the previous winter NAOI, specifically for the JFM quarter. Unlike the results discussed in the study on the SSTA dipole by Muñoz et al. (2010), this work shows a stronger DM connection with NAO than with ENSO (Table 1). This may be due to the fact that the DM is an air-sea coupled pattern (it includes coupled surface wind anomalies along with the CS&GM SSTA).

Table 1
Correlations between the Dipole Index, the MCA Index, the March-April timeseries of the SSTA in the CS and GM (boxed areas defined in Fig. 1c), and the zonal wind (U) in the CS with the indices NAOI, ONI, and TNA for the specified quarters. The correlations calculated considering only the positive and negative DM years are in parentheses. Only results above 95% confidence level are shown.

March-April	JFM NAOI	JFM ONI	MJJ TNAI
Dipole Index	-0.73 (-0.92)	0.58 (0.75)	0.64 (0.78)
MCA Index	-0.67 (-0.84)	0.54 (0.75)	0.58 (0.80)
CS SSTA	(-0.76)	0.75 (0.80)	0.40 (0.61)
GM SSTA	0.65 (0.77)	(-0.55)	-0.42 (-0.61)
CS U	-0.47 (-0.82)	0.40	0.61 (0.77)

In addition to the NAO and ENSO, the PNA teleconnection pattern was considered, given the significant GPH anomalies found around its origin region, associated with the DM development (Figs. 4–5). Thereby, the correlations of the Dipole Index were found significant only with the March (R = 0.69) and April (R = 0.63) PNAI, but these do not provide much predictive skill for the DM. Although the PNA is a natural internal mode of climatic variability, it is also strongly influenced by ENSO, so that the positive phase of the PNA pattern tends to be associated with El Niño, and the negative phase tends to be associated with La Niña (Trenberth et al. 1998; Hurrell 2003). Thus, the correlation of the Dipole Index with PNAI agrees with previous knowledge since it presents the same sign as the correlation with ONI.

The positive correlation of MCA Index with ONI is consistent with the results for the coupling with the wind STD (Fig. 1), since the positive (negative) phase of ENSO has been associated with an increase (decrease) in the frequency of the mid-latitude systems that cross the CS&GM region, such as cold surges and migratory high pressures (e.g., Hernández 2002; Romero-Centeno et al. 2003). In other words, El Niño contributes to an increase in spring wind variability over the CS&GM region that favors the development of the DM positive phase. On the contrary, the significant negative correlation found with the NAOI suggests that a positive (negative) phase of NAO would be favoring a decrease (increase) in this

atmospheric variability; namely, greater (less) stability and persistence in the magnitude and direction of the trade winds -highly consistent with the NASH position and intensity (Wang 2007)-, supporting the development of the negative (positive) DM.

For a deeper understanding, analogous correlations were computed for the SST and wind components anomalies, separately, and for CS and GM. Significant outcomes were obtained with the SSTA in both basins and only with the zonal wind in CS (Table 1). The correlations of GM SSTA with the NAOI, ONI, and TNAI are of opposite sign to those obtained for the CS SSTA, which denotes the tendency to a dipole structure in the spring SSTA field over the CS&GM in response to large-scale forcings. Overall, considering only the years with positive and negative DM, the correlations result in higher values (inside parentheses in Table 1), confirming the high sensitivity of the DM to remote influences.

Previously, we detected that the wind-SST anomalies associated with the DM life cycle seem to form part of a large-scale pattern and could remain on the TNA for several months after spring (Fig. 3). The highest correlations of DM with the TNAI following the DM months were found for the May-June-July quarter (MJJ, Table 1), although significant positive values persist throughout the rest of the summer (not shown). The positive correlation of the CS zonal wind with the TNAI stands out, which reinforces the well-documented close relationship between the weakening (strengthening) of the trade winds and the SST warming (cooling) in the TNA (e.g., Kushnir 1994; Enfield and Mayer 1997). Such mechanism, present over most of the deep tropics, has been referred to as Wind-Evaporation-SST (WES) feedback and it is mainly governed by the impact of winds on the latent heat flux (Xie and Philander 1994; Xie 1999; Saravanan and Chang 2004; Mahajan 2008). At mid and higher latitudes, changes in the advection of air masses, that cause changes in the air-sea temperature and humidity gradients, are important too (Seager et al. 2000).

For both extreme phases of NAO and ENSO, we performed composite analyses of the anomalous wind and SST fields (Figs. 9 and 10, respectively). Composites of wind anomalies confirm that, inside the CS, the trade winds show a significant change between opposite phases of the NAO (Fig. 9), with also a significant signal in the resulting wind speed. This result agrees with Wang (2007), but it differs from Chang and Oey (2013) who found insignificant correlations and a weak influence of NAO on the interannual changes of the CS trade winds since 1980.

However, comparing the years of El Niño versus La Niña, the wind over the CLLJ region presents significant anomalies only during the El Niño phase (Fig. 9). As mentioned at the beginning of this subsection, of the wind components for the CS and GM, only the CS zonal wind anomalies showed a significant correlation with the NAO and ENSO of the previous winter, especially with the former; and the correlation with the JFM NAOI is notably higher when only the years with extreme DM are considered (Table 1). This analysis is consistent with the GM wind anomaly patterns displayed in Fig. 9, where a sufficiently robust response to the phase change of the NAO and ENSO is not observed, like that found between opposite DM phases (Fig. 2).

By contrast, the SSTA associated with the extreme phases of the NAO are more significant in the GM (in general they are above the 95% level) than in the CS, indicating that the NAO may have a greater effect on the SSTA of the former (Fig. 10). This could be partially linked to the large-scale tripole pattern in the North Atlantic SSTA or to an indirect response associated with the CLLJ variability, both induced by the NAO. Although the physical mechanisms that justify this relationship are not clear, Wang (2007) found a significant correlation between the intensity of the CLLJ in January-February and the SSTA in the GM. Also, it is known that the northward branch of the CLLJ advects moisture from the warm CS across the GM modulating climate variability in that region (Cook and Vizy 2010; Durán-Quesada et al. 2010; Garcia-Martinez and Bollasina 2020). On the contrary, the CS SSTA are more sensitive to the ENSO variability. In this region, significant SSTA completely change the sign between the extreme phases of ENSO (Fig. 10). The GM also presents significant SSTA mainly during the El Niño phase. The apparent polarized SSTA response to these teleconnection patterns at the CS and the GM is also evident in the results provided in Table 1. Nevertheless, ENSO, like the NAO, shows a significant correlation with the SSTA of both subdomains in the DM extreme years (Table 1, values in parentheses).

As illustrated in Figs. 2, 9, and 10, the spatial patterns of the wind and SST anomalies during the DM positive phase are quite comparable to those in the springs after winters of El Niño, and somewhat similar to those springs following a negative NAO, although the anomaly amplitudes are much smaller for the last one. In contrast, the patterns of the negative DM have a higher resemblance with those following a positive NAO winter, but not much with those after a La Niña winter. Figure 11 shows the dispersion of the DM phases based on the ONI and NAOI. Here, the asymmetric relation of the DM with the extremes phases of both teleconnection events is evidenced. The scatters of the positive DM are mostly located in the upper-left quadrant; therefore, this phase tends to occur after an El Niño event during the previous winter under negative NAO conditions. On the other hand, the scatters of the negative DM are concentrated around the lower and medium right sides of the graphic. Hence, the DM negative phase seems to be more sensitive to a positive NAO during the previous winter, under La Niña or neutral conditions of ENSO.

The neutral phases of DM usually occur under neutral or negative NAO in combination with or very close to La Niña conditions (Fig. 11). That is, in the absence of both, El Niño and a positive NAO, during the antecedent winter it is unlikely that an extreme phase of the DM will develop; only 3 of the 14 DM extreme phases do not meet this criterion. The distribution of the scattered points suggests that simultaneous phases of opposite signs of NAO and ENSO during the previous winter, tend to reinforce the DM anomalies. Considering the position in the graph of 10% of the most positive and negative DM cases, the link of the positive DM with El Niño and the negative DM with a positive NAO appears more robust; in both cases, the effect is strengthened by the concomitance of a negative NAO and La Niña, respectively.

Otherwise, using the FMA quarter as representative of the persistent anomaly patterns, the GPH anomaly composites for six cases were explored and compared: for DM positive and negative years, after both extreme phases of winter NAO, and after a mature El Niño or La Niña events. Figure 12 shows these six GPH composites for 500hPa. Additionally, Figs. S3 and S4 provide the same composites for 300hPa and

850hPa levels, respectively. Overall, GPH patterns for opposite phases of the DM, NAO, and ENSO present fairly specular anomalies in each case; to a lesser extent for El Niño/La Niña, considering the smaller magnitude and spatial coverage of significant anomalies above the 95% level for La Niña composites.

The GPH composites for DM in Fig. 12 exhibit again the two cores of significant anomalies on both sides of the North American continent, that were identified in Section 3b for the preceding winter (Figs. 4–5). These GPH anomaly patterns with marked changes in each DM phase from the upper to the lower troposphere would modulate the meridional pressure gradient, particularly on the equatorial side of the NASH (Figs. 12, S3, and S4). The negative (positive) GPH anomalies are associated with the weakening (strengthening) of such gradient and a consequent decrease (increase) in the intensity of the trade winds over the TNA, all of which, as it is already explained, favors the positive (negative) phase of the DM.

The GPH composites for positive DM and El Niño display very similar distributions, suggesting the strong modulator role of the equatorial Pacific warming on the DM positive event (Figs. 12, S3, and S4). These large-scale atmospheric patterns present under an El Niño event are in good accordance with many earlier studies (e.g., Alvarado et al. 2001; Ribera and Mann 2002), particularly the great asymmetry observed, at middle and upper troposphere, between the anomalies over the North Pacific at midlatitudes and those over the equatorial and tropical North Pacific. Another of the best-defined atmospheric circulation features during El Niño years is the anomalous low-pressure system located in the vicinities of the southeastern United States (Wallace y Gutzler 1981; Klein et al. 1999). In the case of the springs following La Niña events, the GPH anomaly patterns are slightly significant at the 95% confidence level (Fig. 12). This result implies a small impact of La Niña phase on the GPH variability during the boreal spring, mainly over North America and the North Atlantic basin. Therefore, unlike El Niño, La Niña does not seem decisive to modulate the DM.

Additionally, we found a great resemblance between the GPH anomaly patterns for the positive DM and negative NAO, as well as between the composites of negative DM and positive NAO (Figs. 12, S3, and S4). These pairs of cases reveal significant changes in the NASH region and emphasize that a winter NAO can trigger or enhance the tropospheric anomalies in the North Atlantic side that favor the development of the DM positive or negative phase.

Besides the above comparison of GPH anomalies, we performed a composite analysis of separated phases for the jet stream. Figures S5 and S6 present the jet anomaly patterns analogous to Fig. 7 for the DM, but for opposite phases of NAO and ENSO, respectively. Here, we also found a considerable consistency between the composites of positive DM and the spring following an El Niño event, showing a southward migration of the subtropical jet, increasing the jet core frequency at latitudes around 30°N and across the GM and subtropical North Atlantic. A pattern very similar to this but less significant is also observed for negative NAO. Thus, in addition to the modulation of the trade winds, the anomalous southward shift of the subtropical jet, with the associated alteration of the storm tracks, would be another mechanism by which the relationship between the positive DM and El Niño, and to a lesser extent with the negative NAO, is established.

However, as shown in Figure S6, La Niña does not reflect a significant change in the subtropical jet stream, but the pattern presents a configuration very close to climatology. Likewise, the positive NAO shows almost no significant changes in the jet stream, although some gridpoints with significant positive anomalies in the jet frequency are observed over latitudes between 40° and 50°N (Fig. S5). This response is not as robust as the pattern obtained for the negative DM (Fig. 7). Strictly speaking, the changes in the jet associated with the positive NAO and La Niña seem to be negligible compared with neutral conditions. Notwithstanding, the arguments discussed in this section point to that a positive NAO could contribute to the development of the negative phase of DM, through mechanisms that might involve other systems as the NASH and CLLJ. La Niña, on the contrary, does not influence or, in any case, it has a lesser impact on the development of the negative DM.

4 Summary And Conclusions

The Dipole Mode is a persistent ocean-atmospheric pattern, known as the leading mode of springtime wind-SST coupled variability in the CS&GM (RV19). The dipole consists in SSTA of opposite signs between the CS and the GM. To further study this mode and consider a more dynamical approximation to the atmospheric variability influence on the SSTA evolution, we performed a MCA between anomalies of SST and wind STD. The DM positive (negative) phase implies an increase (decrease) in wind variability during spring. Such wind STD changes entail that the mean wind is not the only variable involved in the mechanisms related to the coupling with SSTA, but there are other processes suggested throughout this study that become important. The consistency between the CCA carried out by RV19 (using the mean wind) and the MCA (using the wind STD) demonstrated the high persistence of the SSTA dipole in the Intra-Americas Seas previously identified by other authors (Muñoz et al. 2010; Liu et al. 2015; Maldonado et al. 2017; Martinez et al. 2020), since this pattern emerges as the first mode in the coupling with the wind variability. The large-scale tropospheric anomalies observed in this study proved that the DM in the CS&GM intrinsically represents a coupled ocean-atmosphere pattern, and it is highly dependent on winter tropical and extratropical atmospheric conditions.

The evolution of the significant wind-SST anomalies associated with the DM from the previous winter through early summer shed light on its close relationship with the equatorial Pacific and the tropical and subtropical North Atlantic variability. GPH anomaly composites and correlations patterns showed significant changes from the upper to lower troposphere in the North Pacific and North Atlantic Oceans. These patterns suggest that the DM arises from variations in the meridional pressure gradient on the equatorial side of the subtropical high pressures belt since the antecedent winter. In this gradient, the significant changes in the NASH circulation and associated low-level winds, are particularly important for the CS&GM climate. The DM also reflects shifts in the latitudinal position of the subtropical jet stream. Thus, during the positive phase of the DM, the meridional GPH gradient and the trades are diminished, the NASH is weakened with its southwestern ridge less extended towards the CS&GM, while the jet is observed more frequently at lower latitudes than its mean position (descending to the northern GM). These atmospheric circulation changes justify the increase in wind direction variance due to disturbance arrivals favoring a more irregular wind field and instabilities. The opposite features apply to the negative

DM: an intense NASH favors more persistent and stable atmospheric conditions, blocking perturbations, in accordance with a reduced wind STD.

The atmospheric conditions explored in this study reveal that different mechanisms act in the CS and the GM to explain the DM interannual variability. In the CS, the zonal wind anomaly superimposed to the prevailing trades generates changes in the wind speed that contribute to SSTA. The strength and east-west excursion of the NASH influence the surface pressure gradient in the CS and the trade winds intensity. These interannual variations impact the CS SST through changes in the air-sea heat fluxes mainly during the DM positive phase. For the negative phase, the anomalies of SST in the CS are weak, and, in turn, the heat fluxes do not show significant anomalies. In the GM, latitudinal shifts of the subtropical jet stream during spring appear to modulate the advection of dry and cold continental air over this region. This could explain better the SSTA in the GM through the thermodynamic mechanism produced by differences in specific humidity and temperature between the atmosphere and the ocean surface. Therefore, on the interannual timescale, the atmospheric circulation anomalies of the NASH and the subtropical jet for the DM extreme phases interact with each other to produce an opposite impact on the SSTA: while the CS experiences a warm-up, the GM faces a cool-down, and conversely.

The DM is also linked to diverse teleconnections and is partially predictable by the remote influences from ENSO and NAO, but not symmetrically for neither of them. The maximum linear correlations of the Dipole Index with the NAOI and ONI were obtained, in both cases, for the previous JFM quarter: negative and stronger with NAOI and positive with ONI. While the SSTA Dipole found by Muñoz et al. (2010) responds more strongly to the combination of a positive PNA and a warm ENSO, this study adds the importance of the winter NAO to influence the coupled wind-SST DM during the next season. Unlike previous studies, as Chang and Oey (2013), here it is evidenced that low-level zonal winds in the CS are significantly correlated with the winter NAO. Furthermore, the SSTA at the GM show a significant response to the NAO phase change, while in the CS they appear to be mainly modulated by ENSO. Despite the apparent polarized response of SSTA to NAO and ENSO in the CS and GM, there could be nonlinearities between each of these teleconnection patterns and the wind-SST anomalies that trigger the DM.

Moreover, the DM showed a clear-cut connection with the TNA SSTA during and after the spring. The maximum correlation of the Dipole Index with the TNAI was obtained for the MJJ quarter. The persistence of the GPH, SST, and winds anomaly signals after the DM months points out the important role that DM variability might be playing to modulate the climate anomalies into CS&GM and adjacent continent throughout the next summer.

The analysis of the relation between the separated phases of DM with both NAO and ENSO indices gave more elements to understand their asymmetric teleconnections over the CS&GM in spring. Positive DM tends to occur after an El Niño winter under negative NAO conditions. The negative phase of DM, on the other hand, responds more to a positive NAO in the previous winter, under La Niña or neutral ENSO conditions. La Niña does not seem to have a great influence on the development of any of the DM phases. In fact, following winters with La Niña, the DM neutral phases prevail. However, the results

indicate that simultaneous opposite signals of both teleconnection patterns in winter tend to reinforce the DM.

NAO and ENSO modulate DM variability through changes in atmospheric circulation patterns. Based on composites of the NAO and ENSO opposite phases, the anomalies in the GPH, high subtropical pressures, and the structure and position of the subtropical jet stream, were compared with the analogous anomaly patterns for the DM extreme phases. El Niño and the negative NAO induce significant anomalies in the GPH field from the upper to lower troposphere, consistent with those of the positive DM. The jet stream pattern linked to El Niño event quite matches the pattern of the positive DM, showing a southward displacement of the jet core from its climatological location. The jet pattern for negative NAO is similar to the positive DM as well, although less robust. Likewise, the GPH anomalies for positive NAO have a high affinity with those associated with the negative DM; but the GPH anomaly patterns obtained for La Niña were less significant in general, although they are not opposed to the DM negative phase. Regarding the subtropical jet, both positive NAO and La Niña do not seem to induce notable changes in the jet stream pattern.

In consequence, El Niño in winter may trigger the positive DM by means of modifications in the meridional pressure gradient that affect the Atlantic trade winds and the NASH. El Niño also modulates the DM through anomalies in the position and structure of the subtropical jet stream, which are reflected in an increment of the wind STD over the region. However, the ENSO forcings in the CS&GM climate during spring interact with the intrinsic variability of the North Atlantic (Giannini et al. 2001).

At the North Atlantic basin, modifications in atmospheric circulation associated with NAO are very consistent with those of the DM patterns, mainly in the NASH region. NAO appears to modulate the DM mostly through mechanisms such as changes in the intensity and extension of the NASH and its influence in the CLLJ. Besides, the strengthening (weakening) of the NASH associated with the NAO seems to impact, indirectly, on the GM SSTA, which may be related to the tripole pattern in the North Atlantic SSTA. A negative NAO implies a weaker NASH and, therefore, a more irregular circulation in the GM region. This would be reflected in the increased wind STD during the positive DM, consistent with an increment of atmospheric disturbances. However, a positive NAO reveals a stronger NASH, which could act as an atmospheric block. Such condition favors a more constant circulation and justifies the decrease in wind STD during the negative DM. Hence, NAO could affect the SSTA in the GM via the modulation of the cold air masses advection coming from the continent, as well as through its influence on the CLLJ variability (Wang 2007). The contribution of the latter to the surface properties of the GM can be due to horizontal advection of humidity (Cook and Vizy 2010), or due to transport fluctuations through the Yucatan Channel (Chang and Oey 2013), which are plausible mechanisms that, however, need to be evaluated in further studies.

The methodology presented in this work, especially the MCA using the wind STD fields, provides a better understanding of the interannual wind-SST coupling in the CS&GM, and supports the physical mechanisms proposed to interpret the atmospheric drivers. This procedure can be applied to other

variability scales and to the analysis of different climatic patterns. This study contributes to a more comprehensive view of the interannual climate variability in the CS&GM, also called the Intra-Americas Seas, strongly influenced by remote forcings. It adds more evidence to the previous grounds on the non-linearity of teleconnection events such as ENSO (Hoerling et al. 1997; Jin et al. 2003) and brings to light the risks of considering the effects of extreme phases as specular, without separately and carefully analyzing both phases.

Declarations

Acknowledgments

This research is a contribution of the Gulf of Mexico Research Consortium (CIGoM), financed by the Mexican National Council for Science and Technology (CONACYT)-Mexican Ministry of Energy-Hydrocarbon Fund, project 201441. Additionally, Geidy Rodríguez-Vera wants to express her gratitude to CONACYT and the Support Program for Postgraduate Studies (PAEP) of the Universidad Nacional Autónoma de México (UNAM) for financing international mobility during this work. This research has been carried out under the institutional support of the Ocean-Atmosphere Interaction Group of the Center for Atmospheric Sciences at UNAM, and the Variability and Reconstruction of Climate Group, at the Department of Physical, Chemical, and Natural Systems, Universidad Pablo de Olavide (Junta de Andalucía, PAIDI group RNM-356). We especially thank the reviewers for their thoughtful comments and suggestions to improve this work.

References

1. Alexander M, Scott J (2002) The influence of ENSO on air-sea interaction in the Atlantic. Geophys Res Lett 29:1701.https://doi.org/10.1029/2001GL014347
2. Alfaro EJ (2007) Uso del análisis de correlación canónica para la predicción de la precipitación pluvial en Centroamérica. Ing Compet 9:33–48. https://doi.org/10.25100/iyc.v9i2.2486
3. Alvarado LF, Fernández W (2001) Variabilidad interanual y estacional de la atmósfera libre sobre Costa Rica durante eventos de El Niño. Top Meteor Oceanogr 8:116–144.
4. Amador JA (1998) A climatic feature of the tropical Americas: The trade wind easterly jet. *Top Meteor Oceanogr* **5**:1-13.
5. Amador JA, Alfaro EJ, Rivera ER, Calderón B (2010) Climatic features and their relationship with tropical cyclones over the Intra-Americas seas. Hurricanes and Climate Change (pp. 149-173). Springer, Dordrecht.
6. Athié G, Candela J, Sheinbaum J, Badan A, Ochoa J (2011) Yucatan Current variability through the Cozumel and Yucatan channels. Ciencias Marinas 37(4A):471–492. https://doi.org/10.15517/rbt.v64i1.23409
7. Barnett TP, Preisendorfer R (1987) Origins and levels of monthly and seasonal forecast skill for United States surface air temperatures determined by canonical correlation analysis. Mon Wea Rev

115:1825–1850. https://doi.org/10.1175/1520-0493(1987)115,1825:OALOMA.2.0.CO;2

8. Barnston AG, Livezey RE (1987) Classification, seasonality and persistence of low-frequency atmospheric circulation patterns. Mon Wea Rev 115(6):1083–1126. https://doi.org/10.1175/1520-0493(1987)115<1083:CSAPOL>2.0.CO;2
9. Bretherton CS, Smith C, Wallace JM (1992) An intercomparison of methods for finding coupled patterns in climate data. J Clim 5:541–560. https://doi.org/10.1175/1520-0442(1992)005,0541:AIOMFF.2.0.CO;2
10. Chang YL, Oey LY (2013) Coupled response of the trade wind, SST gradient, and SST in the Caribbean Sea, and the potential impact on Loop Current's interannual variability. J Phys Oceanogr 43:1325–1344. https://doi.org/10.1175/JPO-D-12-0183.1
11. Chiang JC, Sobel AH (2002) Tropical tropospheric temperature variations caused by ENSO and their influence on the remote tropical climate. J Clim 15(18):2616–2631. https://doi.org/10.1175/1520-0442(2002)015<2616:TTTVCB>2.0.CO;2
12. Chikamoto Y, Tanimoto Y (2005) Role of specific humidity anomalies in Caribbean SST response to ENSO. J Met Soc of Japan Ser. II 83(6):959–975. https://doi.org/10.2151/jmsj.83.959
13. Cook KH, Vizy EK (2010) Hydrodynamics of the Caribbean low-level jet and its relationship to precipitation. J Clim 23:1477–1494. https://doi.org/10.1175/2009JCLI3210.1
14. Curtis S, Hastenrath S (1995) Forcing of anomalous sea surface temperature evolution in the tropical Atlantic during Pacific warm events. J Geophys Res Oceans 100(C8):15835–15847. https://doi.org/10.1029/95JC01502
15. Curtis S, Gamble DW (2016) The boreal winter Madden-Julian Oscillation's influence on summertime precipitation in the greater Caribbean. J Geophys Res Atm 121(13):7592–7605. https://doi.org/10.1002/2016JD025031
16. Dee DP, Uppala SM, Simmons AJ, Berrisford P, Poli P, Kobayashi S et al (2011) The ERA-Interim reanalysis: Configuration and performance of the data assimilation system. Quart J Roy Meteor Soc 137:553–597. https://doi.org/10.1002/qj.828
17. Deser C, Alexander MA, Xie SP, Phillips AS (2010) Sea surface temperature variability: Patterns and mechanisms. Annu Rev Mar Sci 2:115–143. https://doi.org/10.1146/annurev-marine-120408-151453
18. Durán-Quesada A, Gimeno L, Amador J, Nieto R (2010) A Lagrangian approach to moisture sources for Central America: Part I moisture sources identification. J Geophys Res. https://doi.org/10.1029/2009JD012455
19. Enfield DB, Mayer DA (1997) Tropical Atlantic sea surface temperature variability and its relation to El Niño–Southern Oscillation. J Geophys Res 102:929–945. https://doi.org/10.1029/96JC03296
20. Enfield DB, Lee SK, Wang C (2006) How are large western hemisphere warm pools formed? Prog Oceanogr 70(2-4):346–365. https://doi.org/10.1016/j.pocean.2005.07.006
21. Fallas-López B, Alfaro EJ (2012) Uso de herramientas estadísticas para la predicción estacional del campo de precipitación en América Central como apoyo a los Foros Climáticos Regionales. 2:

Análisis de Correlación Canónica. Rev Climatol 12:93–105

22. García-Martínez IM, Bollasina MA (2020) Sub-monthly evolution of the Caribbean Low-Level Jet and its relationship with regional precipitation and atmospheric circulation. Clim Dyn 1–18. https://doi.org/10.1007/s00382-020-05237-y
23. Giannini A, Cane MA, Kushnir Y (2001) Interdecadal changes in the ENSO teleconnection to the Caribbean region and the North Atlantic Oscillation. J Clim 14:2867–2879. https://doi.org/10.1175/1520-0442(2001)014,2867:ICITET.2.0.CO;2.
24. Handoh IC, AJ Matthews, GR Bigg, Stevens DP (2006) Interannual variability of the tropical Atlantic independent of and associated with ENSO: Part I. The North Tropical Atlantic. Int J Climatol, 26, 1937-1956. https://doi.org/10.1002/joc.1343.
25. Hernández B (2002) El Niño-Oscilación del Sur (ENOS) y los frentes fríos que arriban a la región occidental cubana. Investigaciones marinas 30:3–19
26. Hoerling MP, Kumar A, Zhong M (1997) El Niño, La Niña, and the nonlinearity of their teleconnections. J Clim 10(8):1769–1786. https://doi.org/10.1175/1520-0442(1997)010<1769:ENOLNA>2.0.CO;2
27. Hurrell JW, Kushnir Y, Ottersen G, Visbeck M (2003) An overview of the North Atlantic oscillation. Geophys Monogr Amer Geophys Union 134:1–35. https://doi.org/10.1029/134GM01.
28. Jin FF, An SI, Timmermann A, Zhao J (2003) Strong El Niño events and nonlinear dynamical heating. Geophys Res Lett 30(3):20–1. https://doi.org/10.1029/2002GL016356
29. Kalnay E, Kanamitsu M, Kistler R, Collins W, Deaven D, Gandin L et al (1996) The NCEP/NCAR 40-year reanalysis project. Bull Amer Meteor Soc 77(3):437–472. https://doi.org/10.1175/1520-0477(1996)077<0437:TNYRP>2.0.CO;2
30. Klein SA, Soden BJ, Lau NC (1999) Remote sea surface temperature variations during ENSO: Evidence for a tropical atmospheric bridge. J Clim 12:917–932. https://doi.org/10.1175/1520-0442(1999)012<0917:RSSTVD>2.0.CO;2
31. Kushnir Y (1994) Interdecadal variations in North Atlantic sea surface temperature and associated atmospheric conditions. J Clim 7(1):141–157. https://doi.org/10.1175/1520-0442(1994)007<0141:IVINAS>2.0.CO;2
32. Lee SK, Mapes BE, Wang C, Enfield DB, Weaver SJ (2014) Springtime ENSO phase evolution and its relation to rainfall in the continental US. Geophys Res Lett 41(5):1673–1680. https://doi.org/10.1002/2013GL059137
33. Liu Y, Lee SK, Enfield DB, Muhling BA, Lamkin JT, Muller-Karger FE, Roffer MA (2015) Potential impact of climate change on the Intra-Americas Sea: Part-1. A dynamic downscaling of the CMIP5 model projections. J. Mar Syst 148:56–69. https://doi.org/10.1016/j.jmarsys.2015.01.007
34. Mahajan S (2008) Free and forced tropical variability: role of the wind-evaporation-sea surface temperature (WES) feedback. Dissertation, Texas A&M University
35. Mahajan S, Saravanan R, Chang P (2010) Free and forced variability of the tropical Atlantic Ocean: Role of the wind–evaporation–sea surface temperature feedback. J Clim 23(22):5958–5977. https://doi.org/10.1175/2010JCLI3304.1

36. Maldonado T, Alfaro E, Rutgersson A, Amador J (2017) The early rainy season in Central America: the role of the tropical North Atlantic SSTs. Int J Climatol 37(9):3731–3742. https://doi.org/10.1002/joc.4958
37. Martinez C, Kushnir Y, Goddard L, Ting M (2020) Interannual variability of the Early and Late-Rainy Seasons in the Caribbean. Clim Dyn 1–21. https://doi.org/10.1007/s00382-020-05341-z
38. Muñoz E, Wang C, Enfield DB (2010) The Intra-Americas springtime sea surface temperature anomaly dipole as fingerprint of remote influences. J Clim 23:43–56. https://doi.org/10.1175/2009JCLI3006.1
39. Muñoz E, Enfield DB (2011) The boreal spring variability of the Intra-Americas low-level jet and its relation with precipitation and tornadoes in the eastern United States. Clim Dyn 36:247–259. https://doi.org/10.1007/s00382-009-0688-3
40. Peña-Ortiz C, Gallego D, Ribera P, Ordonez P, Alvarez-Castro MC (2013) Observed trends in the global jet stream characteristics during the second half of the 20th century. J Geophys Res Atm 118(7):2702–2713. https://doi.org/10.1002/jgrd.50305
41. Rayner NAA, Parker DE, Horton EB, Folland CK, Alexander LV, Rowell DP et al (2003) Global analyses of sea surface temperature, sea ice, and night marine air temperature since the late nineteenth century. J Geophys Res Atm 108(D14). https://doi.org/10.1029/2002JD002670
42. Reding PJ (1992) The Central American cold surge: An observational analysis of the deep southward penetration of North American cold fronts. Dissertation, Texas A&M University
43. Reynolds RW, Smith TM, Liu C, Chelton DB, Casey KS, Schlax MG (2007) Daily high-resolution-blended analyses for sea surface temperature. J Clim 20:5473–5496. https://doi.org/10.1175/2007JCLI1824.1
44. Ribera P, Mann ME (2002) Interannual variability in the NCEP reanalysis 1948–1999. Geophys Res Lett 29(10):132-1.https://doi.org/10.1029/2001GL013905
45. Riehl H (1962) Jet streams of the atmosphere. Department of Atmospheric Science, Colorado State University. Tech Rep 32
46. Rodríguez-Vera G, Romero-Centeno R, Castro CL, Castro VM (2019) Coupled interannual variability of wind and sea surface temperature in the Caribbean Sea and the Gulf of Mexico. J Clim 32(14):4263-4280. https://doi.org/10.1175/JCLI-D-18-0573.1
47. Romero-Centeno R, Zavala-Hidalgo J, Gallegos A, O'Brien JJ (2003) Isthmus of Tehuantepec wind climatology and ENSO signal. J Clim 16:2628-2639. https://doi:10.1175/1520-0442(2003)016.
48. Saha S, Moorthi S, Pan HL, Wu X, Wang J, Nadiga S et al (2010) The NCEP Climate Forecast System Reanalysis. Bull Amer Meteor Soc, 91:1015–1057. https://doi.org/10.1175/2010BAMS3001.1
49. Saha S, Moorthi S, Wu X, Wang J, Nadiga S, Tripp P et al (2014) The NCEP Climate Forecast System version 2. J Clim 27:2185–2208. https://doi.org/10.1175/JCLI-D-12-00823.1
50. Saravanan R, Chang P (2000) Interaction between tropical Atlantic variability and El Nino–Southern oscillation. J Clim 13(13):2177–2194. https://doi.org/10.1175/1520-

0442(2000)013<2177:IBTAVA>2.0.CO;2

51. Saravanan R, Chang P (2004) Thermodynamic coupling and predictability of tropical sea surface temperature. Geophys Monogr Ser 147:171–180. https://doi.org/10.1029/147GM10
52. Seager R, Kushnir Y, Visbeck M, Naik N, Miller J, Krahmann G, Cullen H (2000) Causes of Atlantic Ocean climate variability between 1958 and 1998. J Clim 13(16):2845–2862. https://doi.org/10.1175/1520-0442(2000)013<2845:COAOCV>2.0.CO;2
53. Schultz DM, Bracken WE, Bosart LF (1998) Planetary-and synoptic-scale signatures associated with Central American cold surges. Mon Wea Rev 126(1):5–27. https://doi.org/10.1175/1520-0493(1998)126<0005:PASSSA>2.0.CO;2
54. Taylor MA, Enfield DB, Chen AA (2002) Influence of the tropical Atlantic versus the tropical Pacific on Caribbean rainfall. J Geophys Res Oceans 107(C9):1–14. https://doi.org/10.1029/2001JC001097
55. Trenberth KE, Branstator GW, Karoly D, Kumar A, Lau NC, Ropelewski C (1998) Progress during TOGA in understanding and modeling global teleconnections associated with tropical sea surface temperatures. J Geophys Res Oceans 103(C7):14291–14324. https://doi.org/10.1029/97JC01444
56. Wallace JM, Gutzler DS (1981) Teleconnections in the geopotential height field during the Northern Hemisphere winter. Mon Wea Rev 109:784–812. https://doi.org/10.1175/1520-0493(1981)109<0784:TITGHF>2.0.CO;2
57. Wang C, Enfield DB (2001) The tropical Western Hemisphere warm pool. Geophys Res Lett 28:1635–1638. https://doi.org/10.1029/2000GL011763
58. Wang C, Enfield DB (2003) A further study of the tropical Western Hemisphere warm pool. J Clim 16:1476–1493. https://doi.org/10.1175/1520-0442-16.10.1476
59. Wang C (2007) Variability of the Caribbean low-level jet and its relations to climate. Clim Dyn 29:411–422. https://doi.org/10.1007/s00382-007-0243-z
60. Xie SP, Philander SGH (1994) A coupled ocean-atmosphere model of relevance to the ITCZ in the eastern Pacific. Tellus A 46(4):340–350. https://doi.org/10.1034/j.1600-0870.1994.t01-1-00001.x

Figures

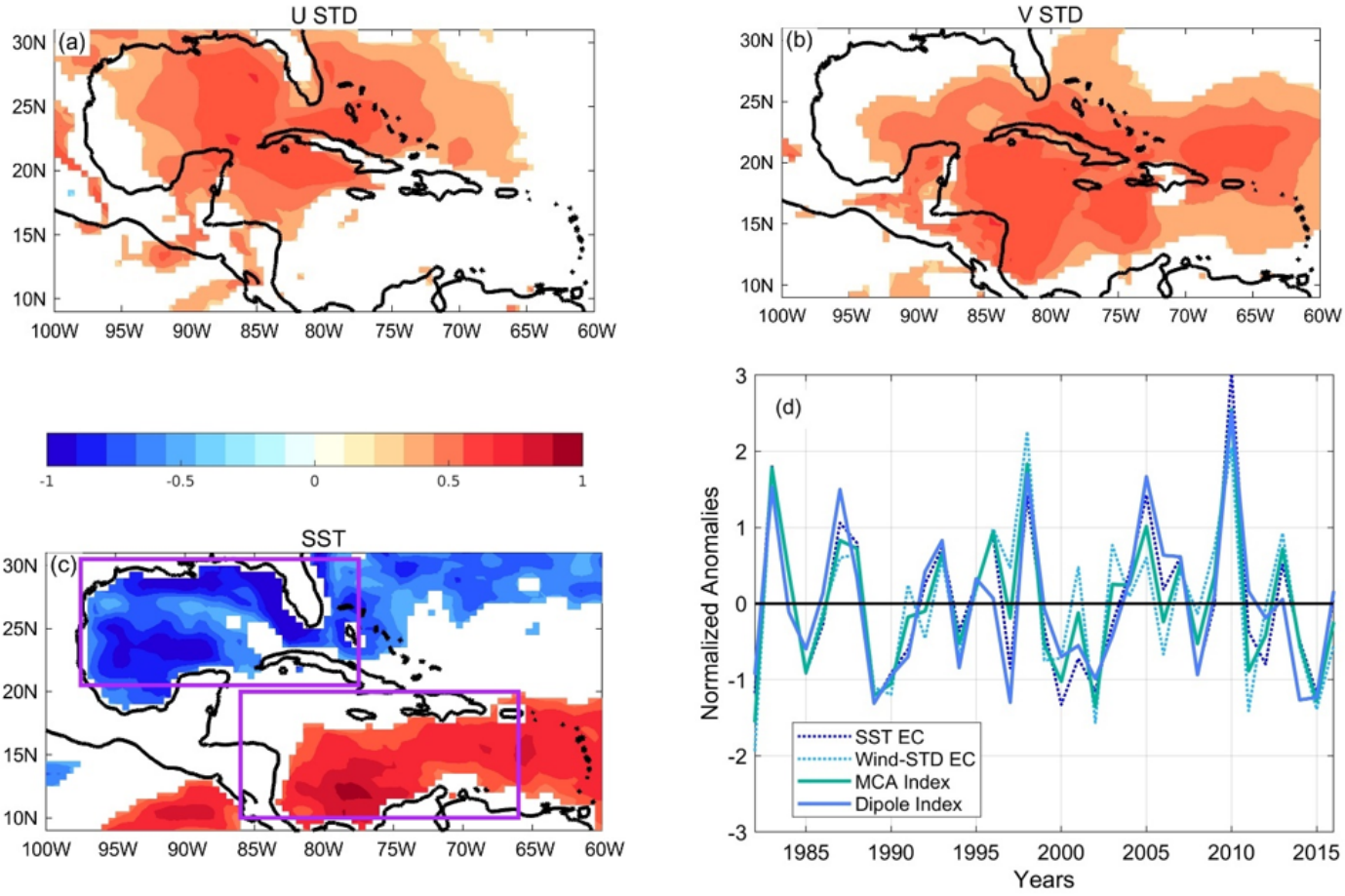

Figure 1

Heterogeneous correlation maps for the first March-April MCA mode for (a) zonal wind STD, (b) meridional wind STD, and (c) SSTA. Color shading indicates the significant correlations at the 95% level. (d) Comparison between the corresponding SST and wind STD expansion coefficients, the MCA Index, and the Dipole Index. Boxed areas in Fig. 1c denote the subdomains defined for the Gulf of Mexico (97.5W-75.5W, 20.5N-30.5N) and the Caribbean Sea (86W-66W, 10N-20N).

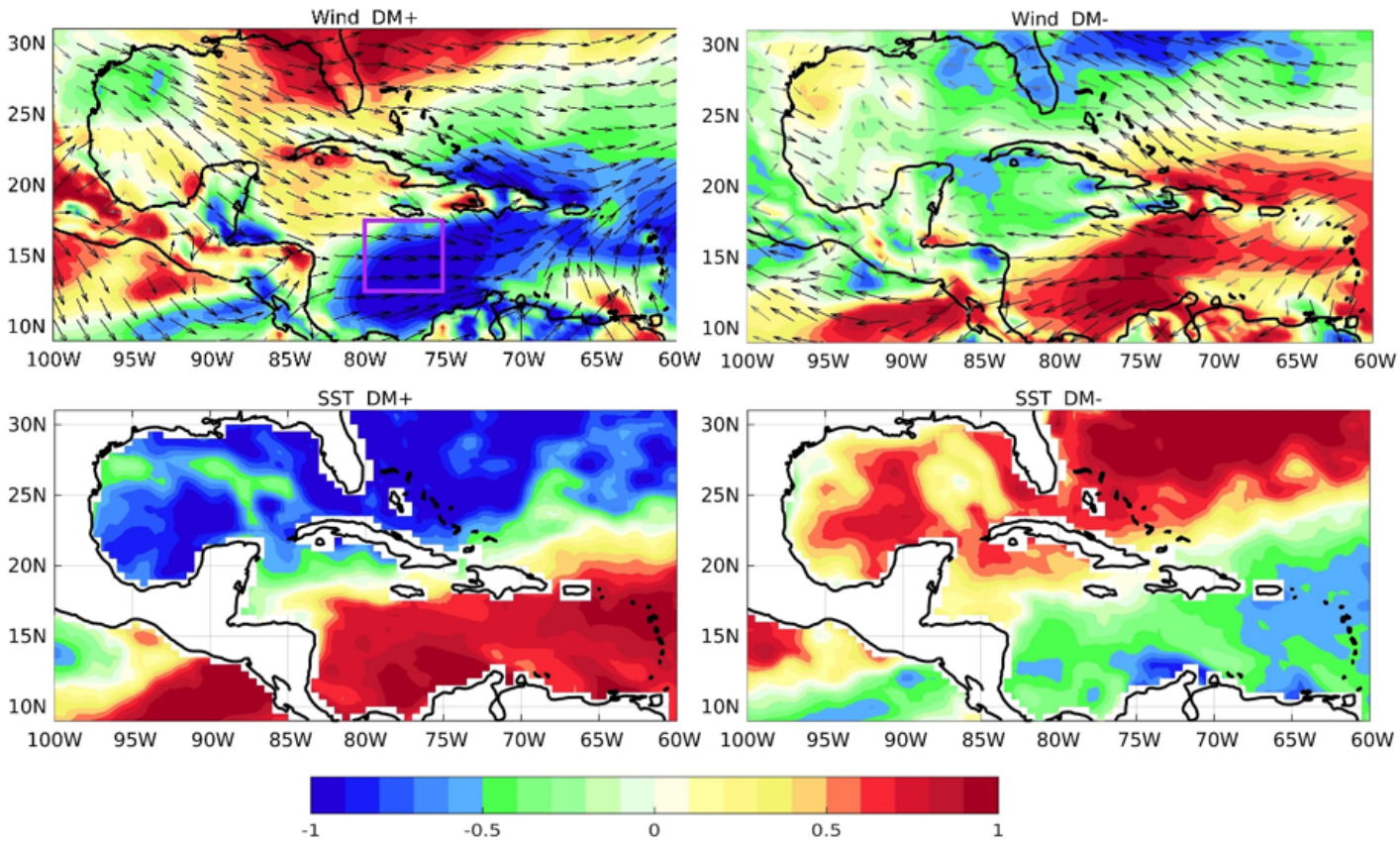

Figure 2

Composites of March-April surface wind (m/s; first row) and SST (°C; second row) standardized anomalies for the DM positive (left column) and negative (right column) phases. In the first row, vectors indicate wind direction anomalies and colors represent wind speed anomalies. Black vectors and color shading above 0.5 (red range) or below -0.5 (blue range) are statistically significant with 95% confidence. Purple box in the first panel comprises the CLLJ core (80W-75W, 12.5N-17.5N) as defined by Amador et al. (2010).

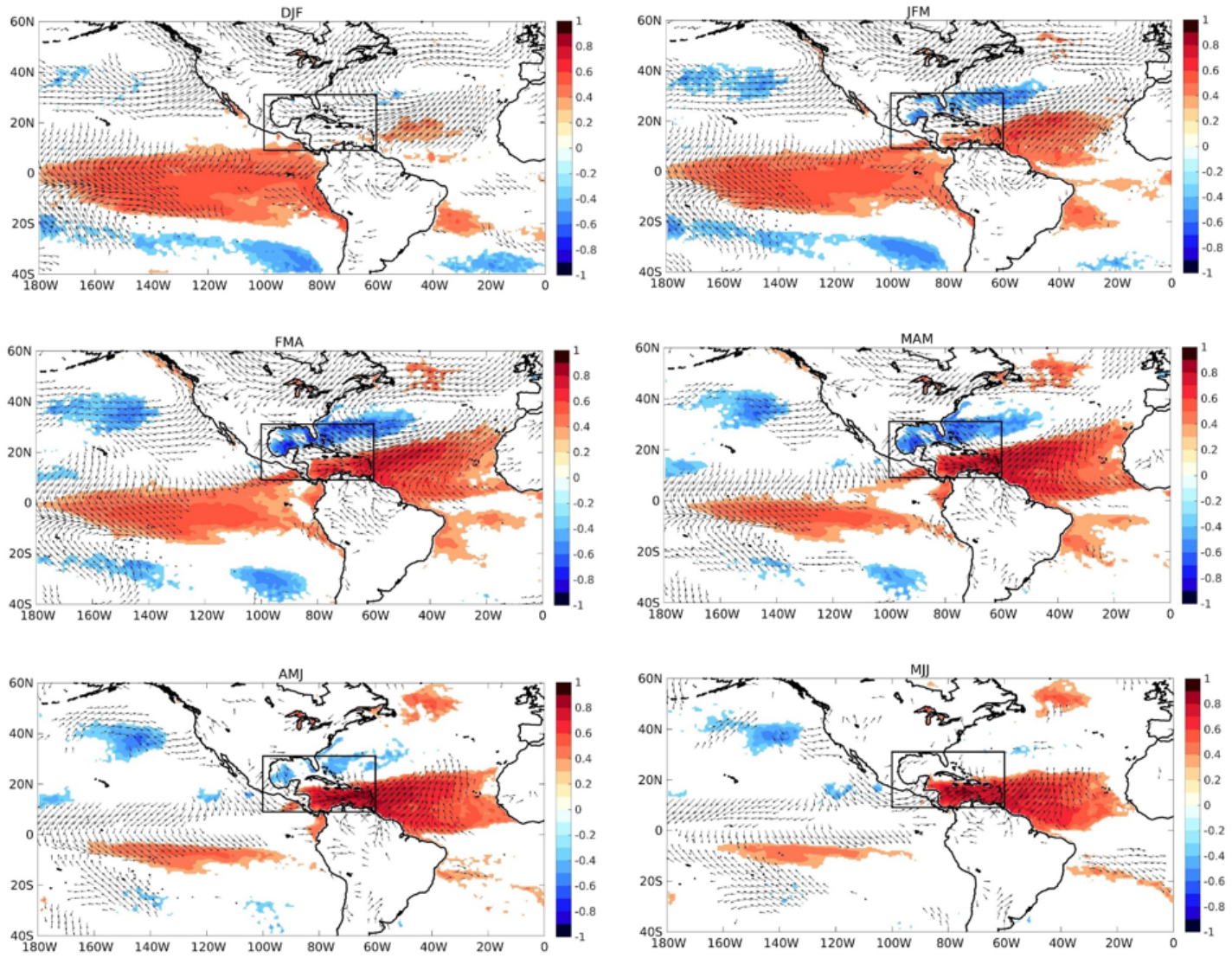

Figure 3

Distributions of SST (°C; shadings) and surface wind (m/s; vectors) anomalies regressed onto the Dipole Index for 3-month running means centered in the months of January (DJF) through June (MJJ). Only grid points where anomalies are significantly correlated (95% confidence level) with the Dipole Index are displayed.

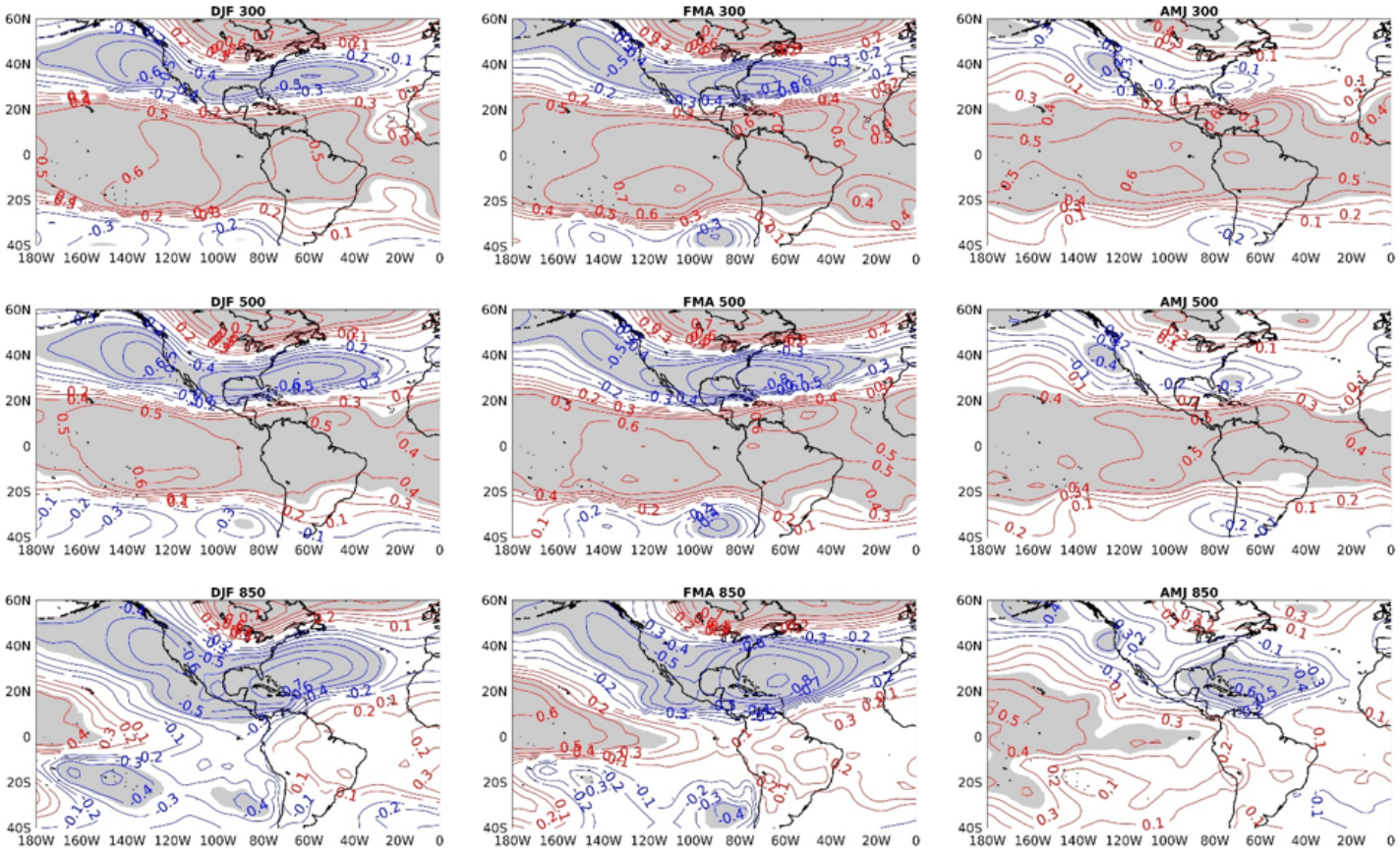

Figure 4

Correlations of the geopotential height anomalies with the Dipole Index (contours) at 300 hPa (first row), 500 hPa (second row), and 850 hPa (third row) for 3-month running mean averages centered on the months of January (DJF), March (FMA), and May (AMJ). Gray shadings correspond to correlations with a 95% confidence level.

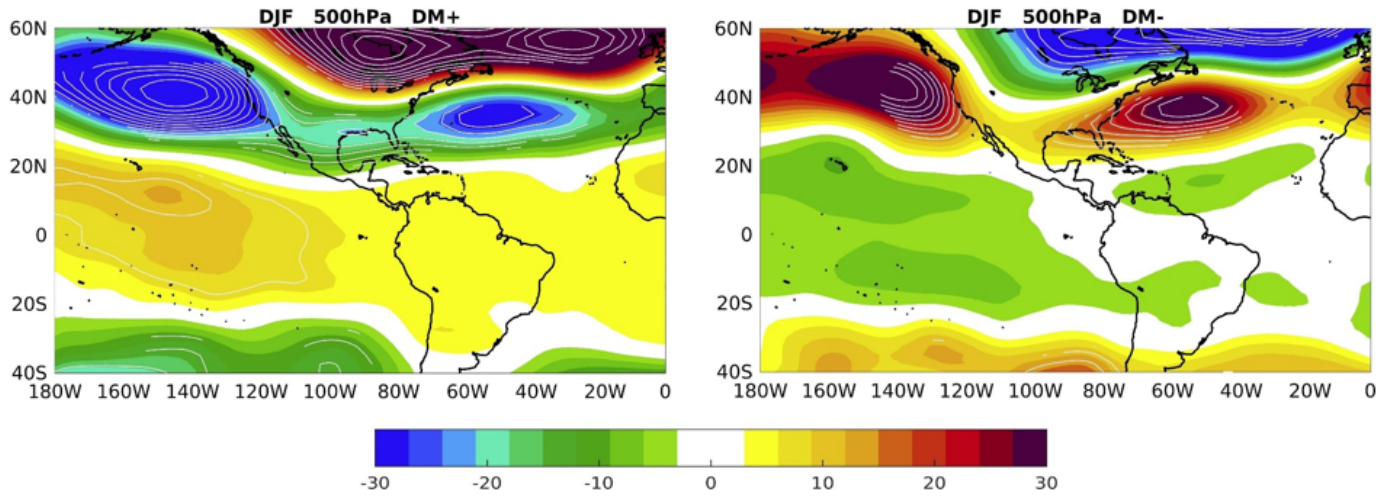

Figure 5

Composites of 500 hPa GPH anomalies for the winter (DJF) prior to the DM positive (left) and negative (right) phases. White contours emphasize areas with 95% confidence level.

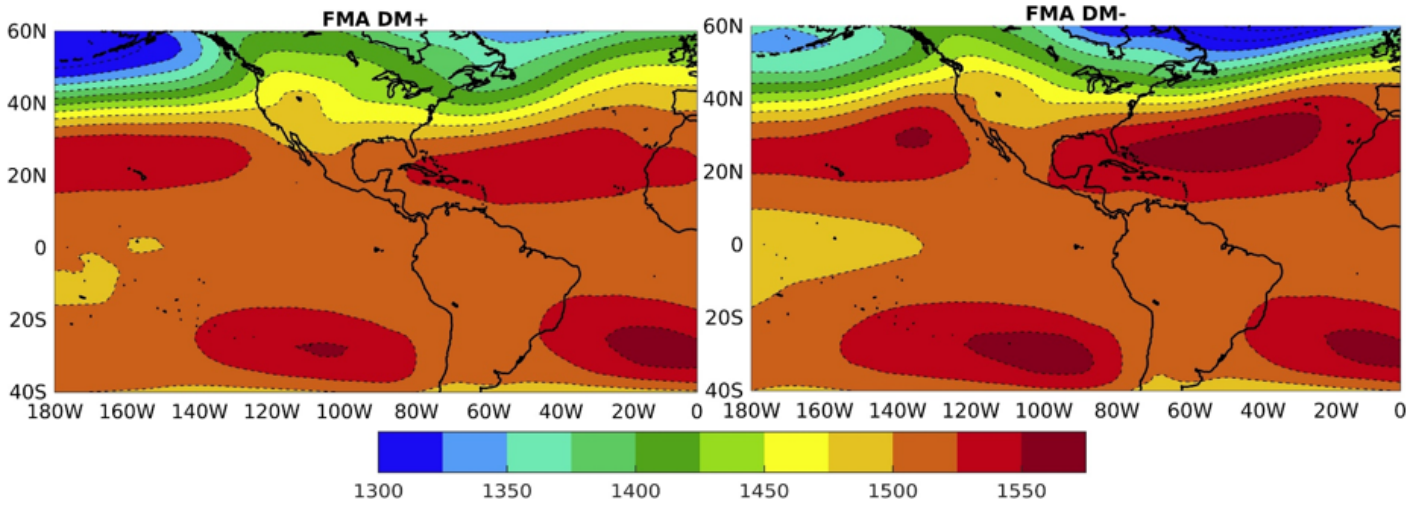

Figure 6

Composites of mean GPH (m) at 850 hPa for FMA considering the DM positive (left) and negative (right) phases.

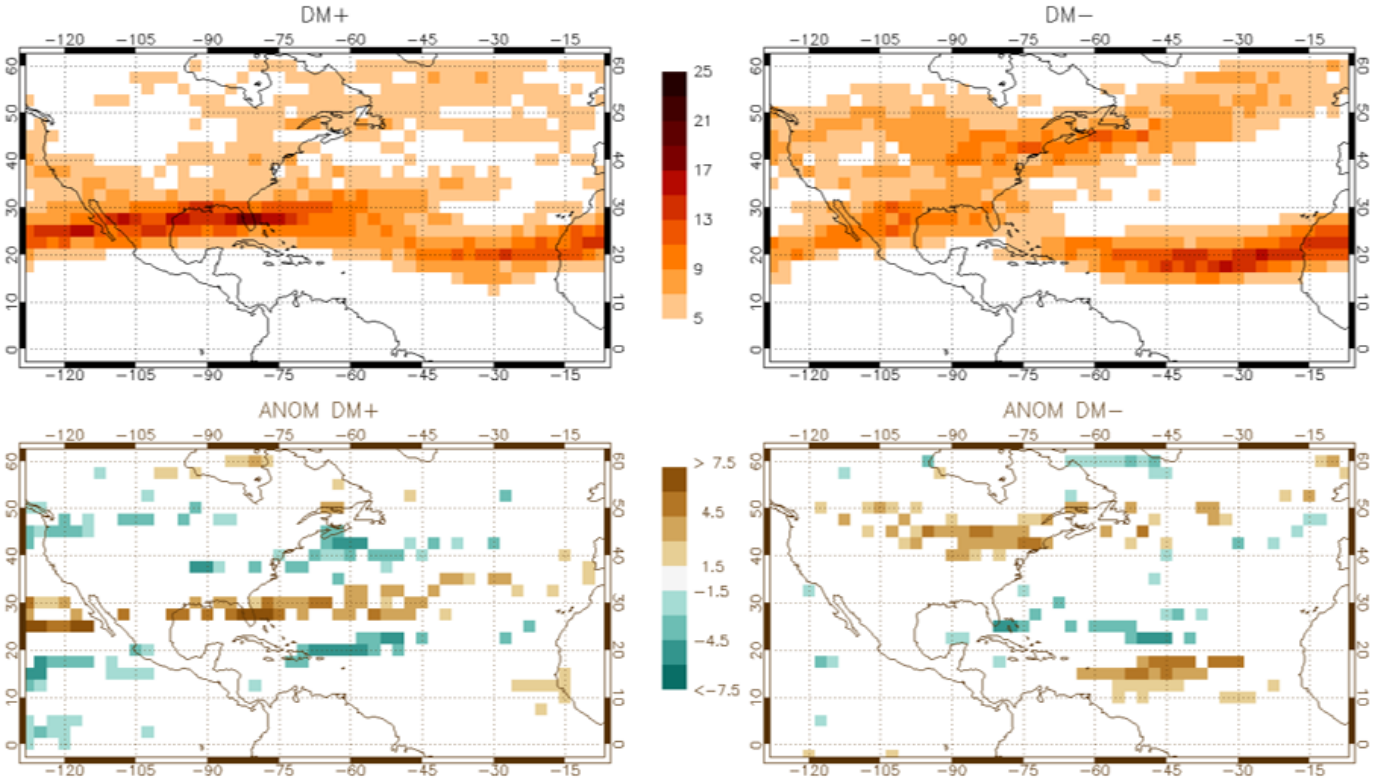

Figure 7

Mean frequency (days/month) of jet streams at each gridpoint during March-April (first row) for the DM positive (left column) and negative (right column) phases, and their differences from the neutral phase

(second row). Only the significant differences with a confidence level of 90% (Monte Carlo non-parametric test with 1000 random repetitions) have been colored.

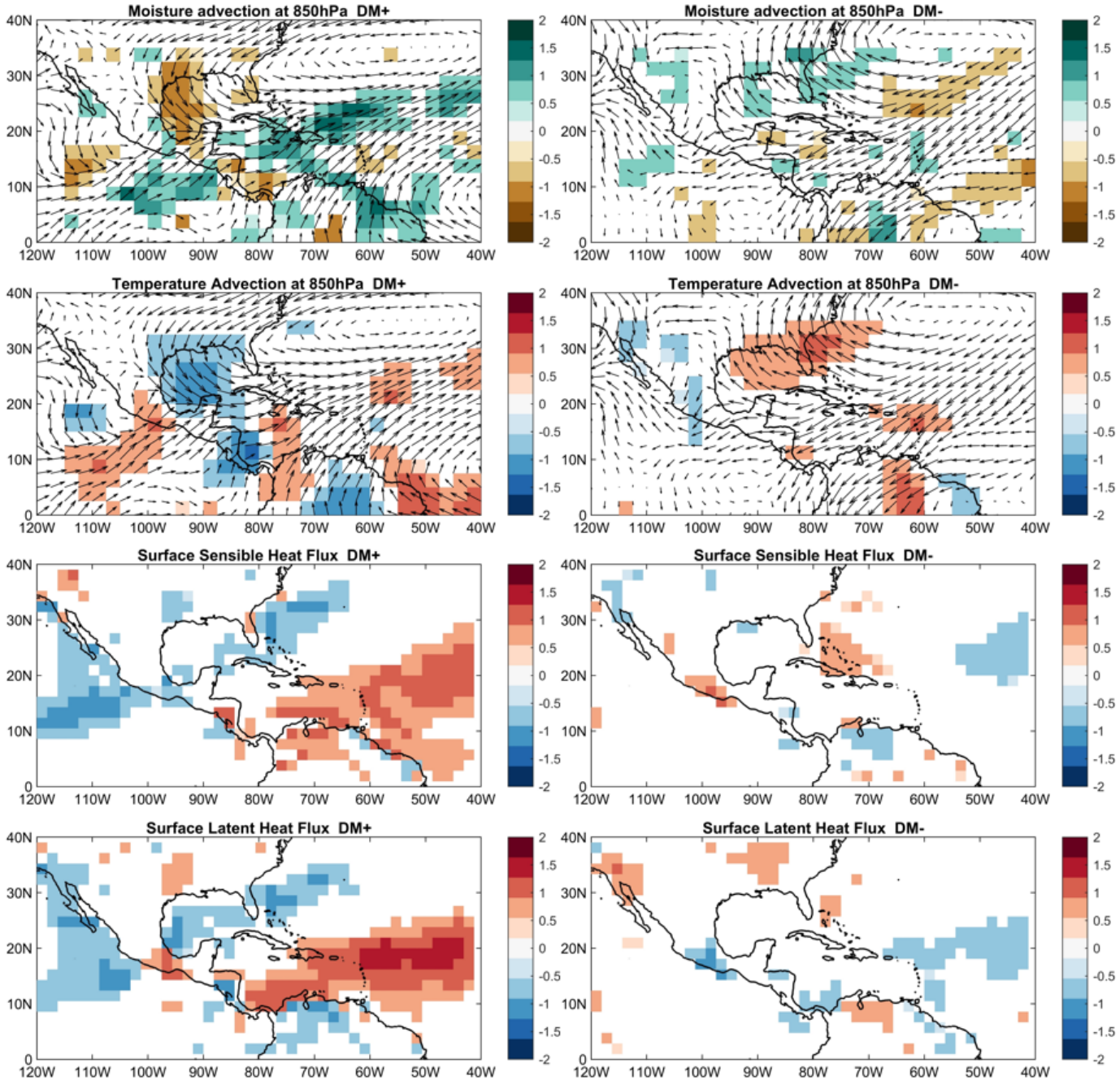

Figure 8

Composites of FMA standardized anomalies of moisture (first row) and temperature (second row) advection at 850hPa, and surface sensible (third row) and latent (fourth row) heat fluxes for DM positive (left column) and negative (right column) phases. In the panels of advection, the anomalies of the wind field at 850hPa have been superimposed. Color shaded areas are significant at the 95% confidence level.

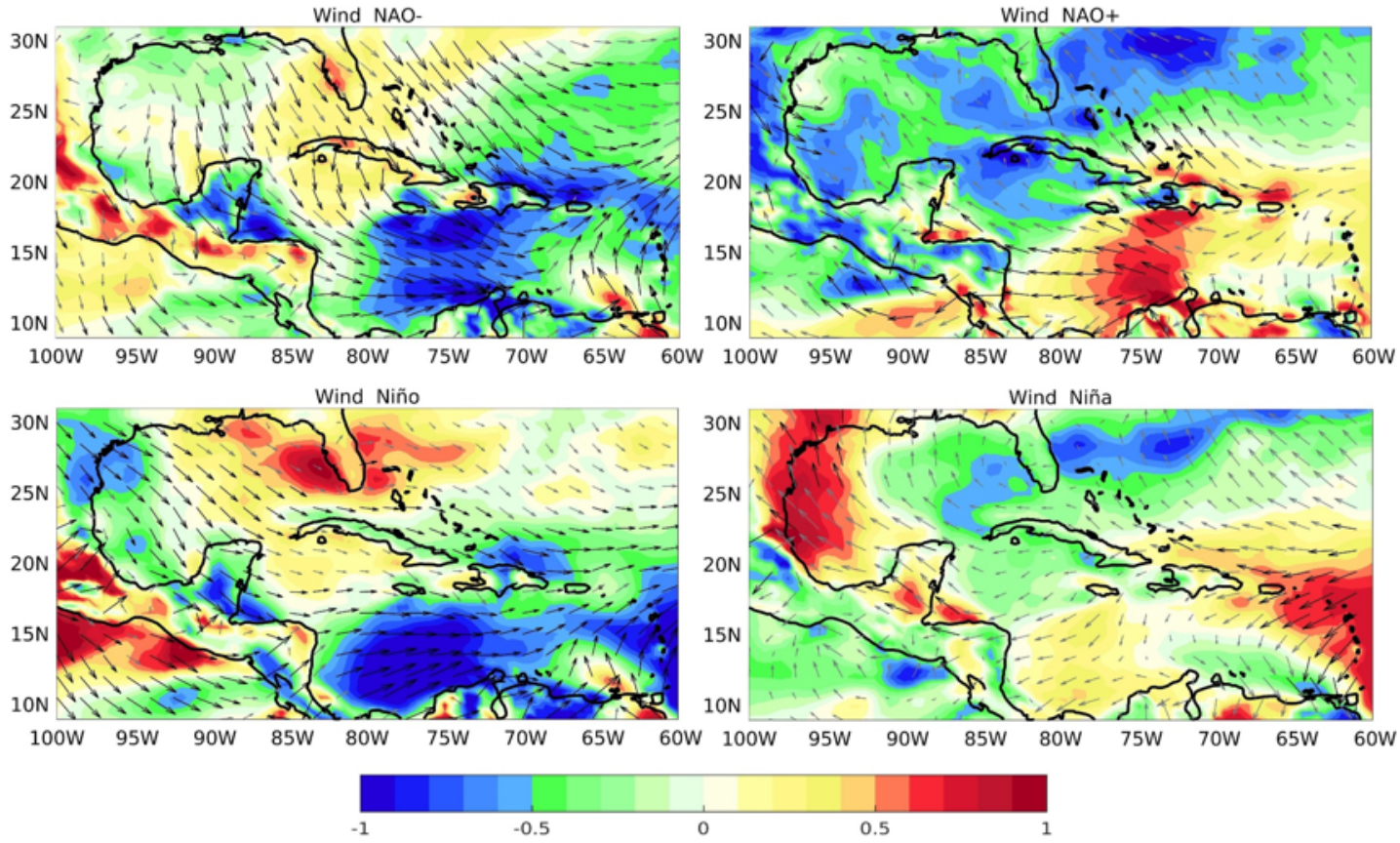

Figure 9

Composites of wind anomalies (m/s) during March-April after winter negative and positive NAO (first row) and El Niño and La Niña (second row). Vectors and colors indicate the direction and magnitude of the wind anomalies, respectively. Black vectors and shadings above 0.5 (red range) or below -0.5 (blue range) are 95% statistically significant.

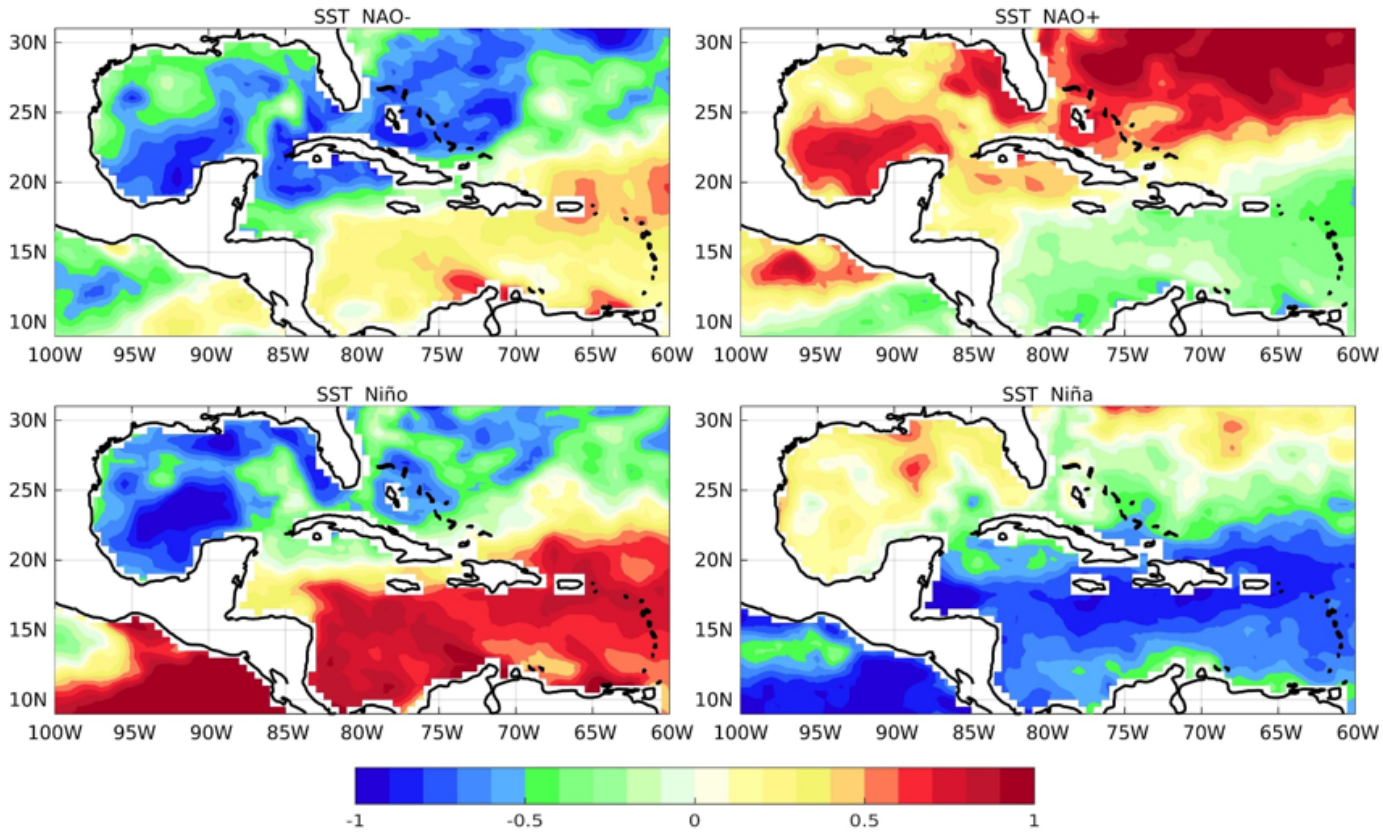

Figure 10

Idem to Fig. 9, but for the SSTA (°C)

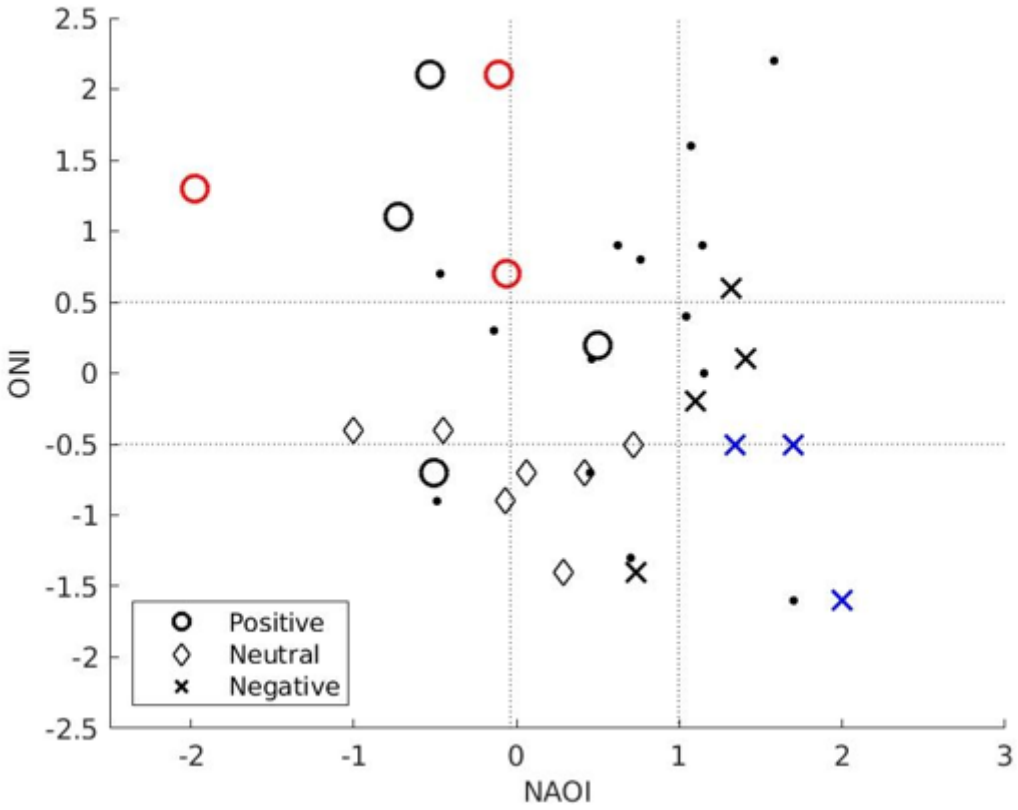

Figure 11

Dispersion of the DM phases with respect to the NAOI (horizontal axis) and ONI (vertical axis) during JFM. Circles represent the positive phases, diamonds the neutral phases, and crosses the negative phases. Black dots do not classify in any of the most representative years of the three mentioned phases. Horizontal dashed lines represent ONI values between ±0.5, while vertical dashed lines indicate the 1/3 and 2/3 quantiles of the NAOI in the 1982-2016 period. 10% of the most positive and negative cases are shown in red and blue, respectively.

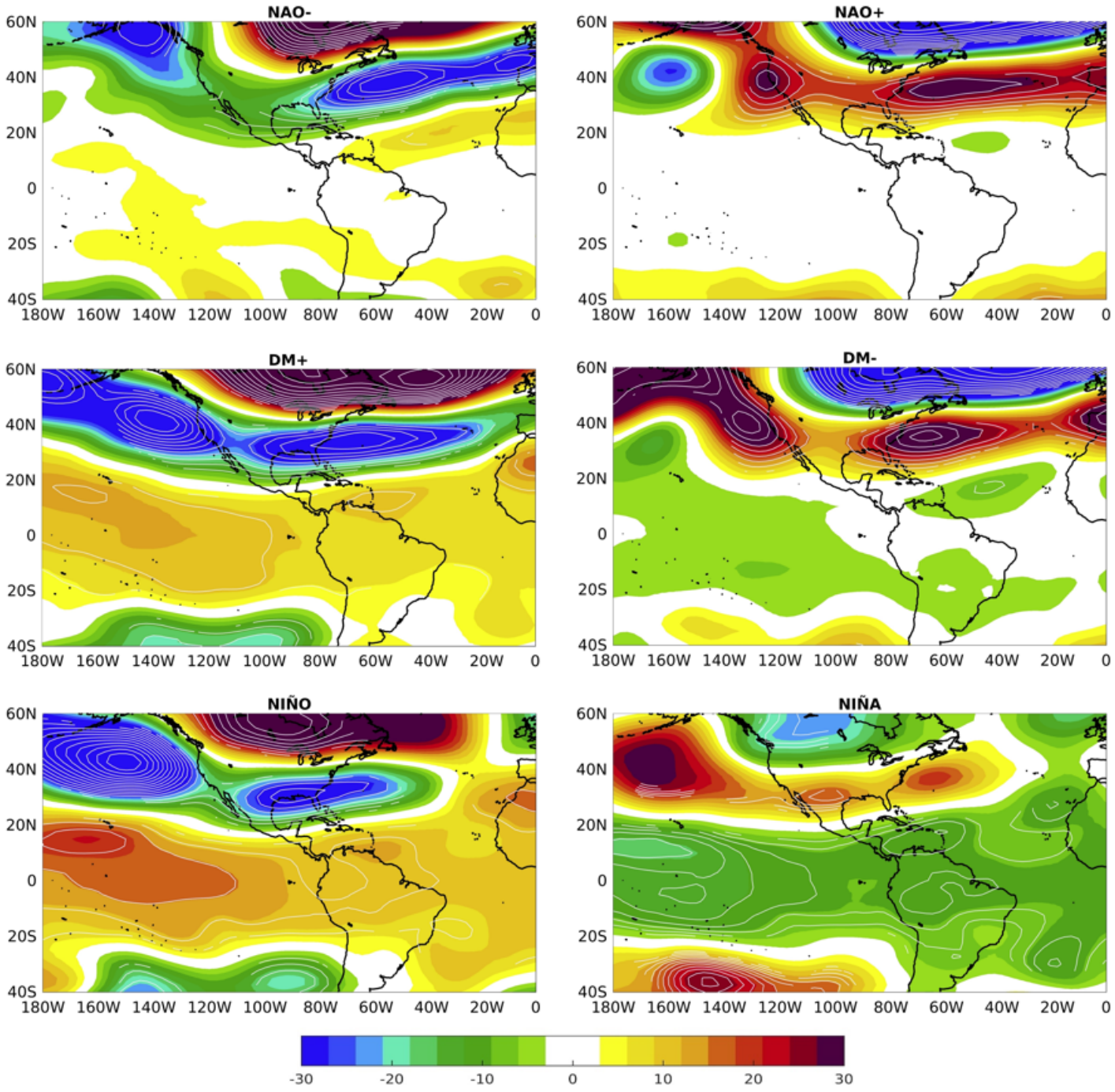

Figure 12

Comparison between composites of 500 hPa GPH anomalies for the spring (FMA): after winters of negative and positive NAO (first row), positive and negative Dipole Mode (second row), and after winters of El Niño and La Niña (third row). White contours emphasize areas with 95% confidence level.

Supplementary Files

This is a list of supplementary files associated with this preprint. Click to download.

- 3Supplementarymaterial.docx